

Supporting Information for:

Effective BPA degradation from water: the integration of bimetallic UiO-66 Ce-Zr

Leidy Marcela Gallo,^a Juan L. Obeso,^{a,b} Nora S. Portillo-Vélez,^c Carlos E. Garduño-

Albino,^c Catalina V. Flores,^a Leonardo Herrera-Zuñiga,^c Alejandro Islas-Jácome,^c

Ricardo A. Peralta^{c*} and Carolina Leyva^{a*}

^aInstituto Politécnico Nacional, Centro de Investigación en Ciencia Aplicada y Tecnología Avanzada, Laboratorio Nacional de Ciencia, Tecnología y Gestión Integrada del Agua, Legaria 694, Col. Irrigación, Miguel Hidalgo, 11500, CDMX, México

^bDivisión de Ingeniería en Sistemas Automotrices, Tecnológico de Estudios Superiores del Oriente del Estado de México (TESOEM), Tecnológico Nacional de México, Estado de México 56400, México.

^cDepartamento de Química, División de Ciencias Básicas e Ingeniería. Universidad Autónoma Metropolitana (UAM-I), 09340, México

Table of contents

S1. Experimental details.....S3
S2. Results and DiscussionsS7
S3. References.....S31

S1. Experimental details

Section S1.

Materials

Zirconium oxychloride octahydrate ($ZrOCl_2 \cdot 8H_2O$), terephthalic acid (BDC), methanol, ethanol, acetone, N-dimethylformamide (DMF), and bisphenol A (BPA) were some of the chemicals we bought from Sigma Aldrich. All chemicals used in this work are of analytical-grade purity and did not require additional purification.

Analytical instruments

To obtain powder X-ray diffraction (PXRD) patterns, a Bruker D2 phaser diffractometer with a Linex eye detector and a Cu-K α 1 radiation anode ($\lambda = 1.5418 \text{ \AA}$) was used. Data were recorded in the $2-40^\circ$ 2θ range with a step scan of 0.02° . A Shimadzu IRTracer-100 spectrometer and KBr pellets were used to obtain Fourier transform infrared (FT-IR) spectra in the $4000-500 \text{ cm}^{-1}$ range, which helped identify the unique bands of each material. Nitrogen adsorption-desorption isotherms were measured by a volumetric method using a Micromeritics ASAP 2020 gas sorption analyzer. The sample mass employed was 65.0 mg. Free space correction measurements were performed using ultra-high purity He gas (UHP grade 5, 99.999% pure). Nitrogen isotherms were measured using UHP-grade Nitrogen. All nitrogen analyses were performed using a liquid nitrogen bath at 77 K. Oil-free vacuum pumps were used to prevent contamination of sample or feed gases. UV-Vis diffuse reflectance spectra were used to determine the band gap energies of all materials, following David and Mott's proposed method based on the Kubelka-Munk equation.¹

Kubelka-Munk function for the Tauc plot graphic.

$$F(R_\infty) = \frac{K}{S} = \frac{(1 - R_\infty)^2}{2R_\infty} \quad (1)$$

$$R_\infty = \frac{R_{sample}}{R_{standard}} \quad (2)$$

$$E_g = h\nu - \frac{(F(R_\infty)h\nu)^\beta}{\beta} \quad (3)$$

Where,

R: reflectance

$\gamma = 2$ for direct allowed transitions

β : semiconductor absorption coefficient

h : Planck's constant

ν : photon's frequency

E_g : band gap energy.

Micrographs were obtained using scanning electron microscopy (SEM) with a JSM-JEOL 7600F microscope to characterize the morphology and size of the prepared samples. X-ray photoelectron spectroscopy (XPS) analyses were conducted using a Thermo Scientific K-alpha X-ray photoelectron spectrometer set to 72 W with a hemispherical analyzer and a monochromator. Survey scans were recorded with a spot size of 400 μm and a fixed pass energy of 200 eV, while high-resolution scans were collected at a pass energy of 20 eV. The spectra were charged and corrected by setting the mainline of the carbon 1s spectrum (adventitious carbon) to 284.8 eV. Spectra analysis was performed using CasaXPS software (version 2.3.14). The Shirley method was used to subtract spectral backgrounds, and the same CasaXPS program carried out curve-fitting procedures and elemental quantifications.

Photocatalytic tests for Bisphenol A degradation

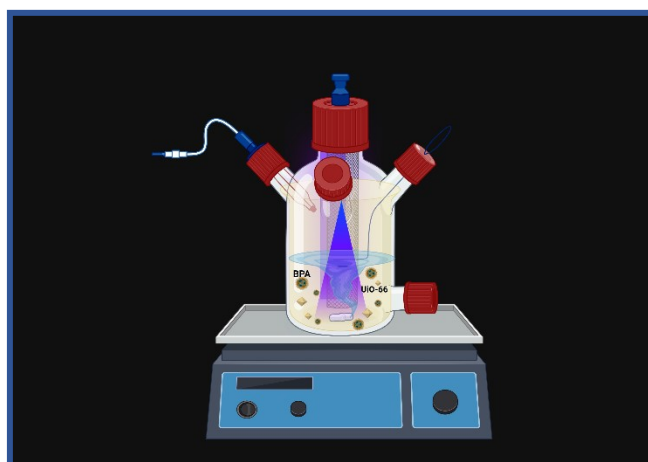


Figure S1. Schematic representation of the photocatalytic process.

Kinetic degradation experiments

Table S1. Kinetics Models for the BPA Degradation		
Kinetic model	Equation	Parameter
PFO model	$C = C_0 e^{-k_{p1}t}$	<p>C: is the concentration of the contaminant at time t (mg·L)</p> <p>C_0: Initial concentration of the contaminant. (mg·L)</p> <p>k_{p1}: pseudo-first-order rate constant for the kinetic model (mg·L⁻¹·min⁻¹)</p>
PSO model	$C = \frac{C_0}{1 + k_{p2}tC_0}$	<p>C: is the concentration of the contaminant at time t (mg·L)</p> <p>C_0: Initial concentration of the contaminant. (mg·L)</p> <p>k_{p2}: pseudo-second-order rate constant for the kinetic model (mg·L⁻¹·min⁻¹)</p>

S2. Results and Discussions

Synthesis of MOF UiO-66

PXRD

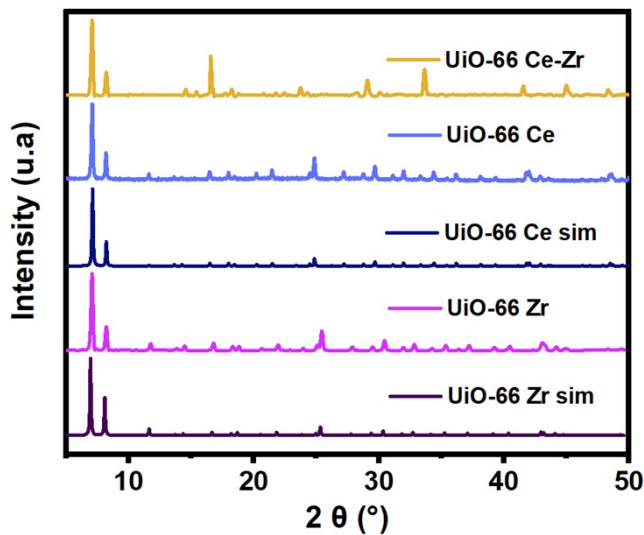


Figure S3. PXRD patterns of MOF UiO-66 Zr simulated, MOF UiO-66 Zr as-synthesized, MOF UiO-66 Ce simulated, MOF UiO-66 Ce as-synthesized and MOF UiO-66 Ce-Zr as-synthesized,

FT-IR

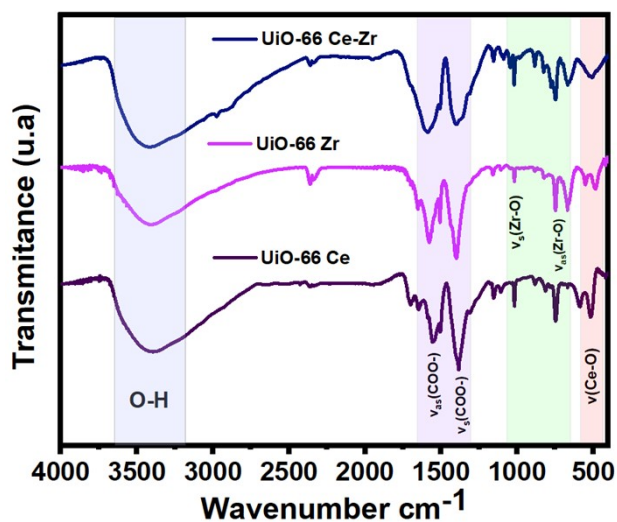


Figure S4. FTIR spectra of synthesized MOFs UiO-66 Ce, UiO-66 Zr and UiO-66 Ce-Zr

SEM-EDS

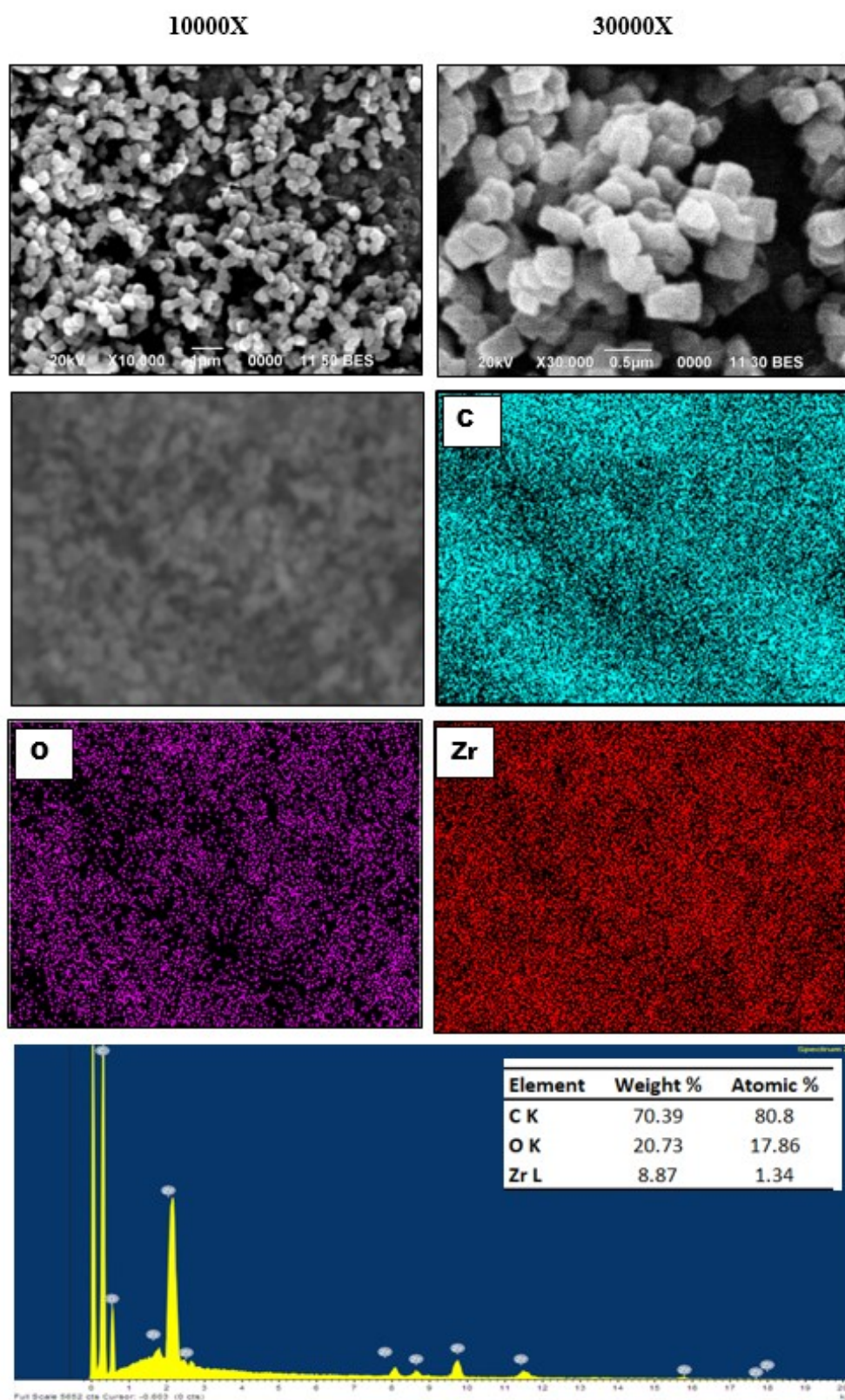


Figure S5. SEM images and SEM-EDS mapping for MOF UiO-66 Zr

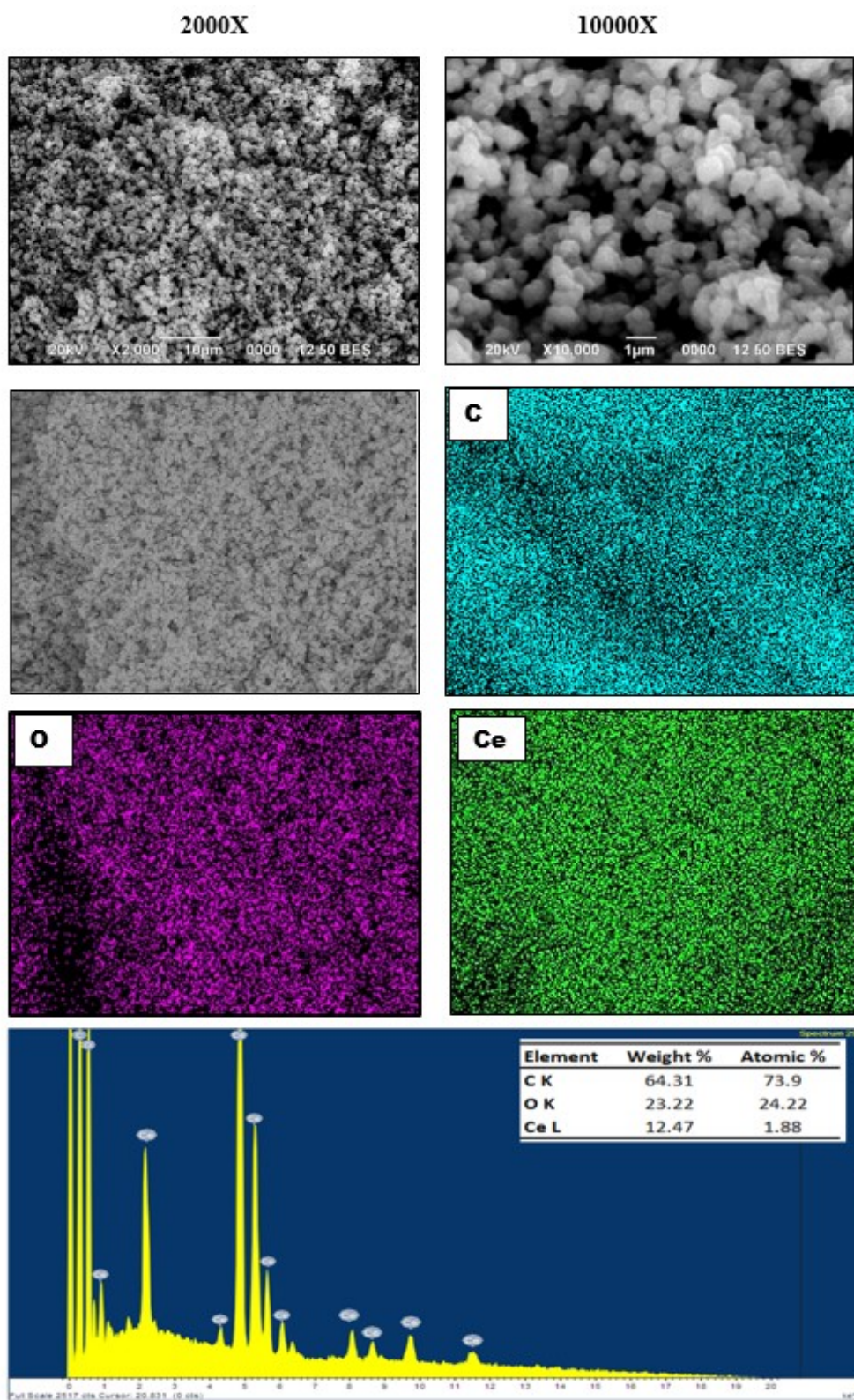


Figure S6. SEM images and SEM-EDS mapping for MOF UiO-66 Ce

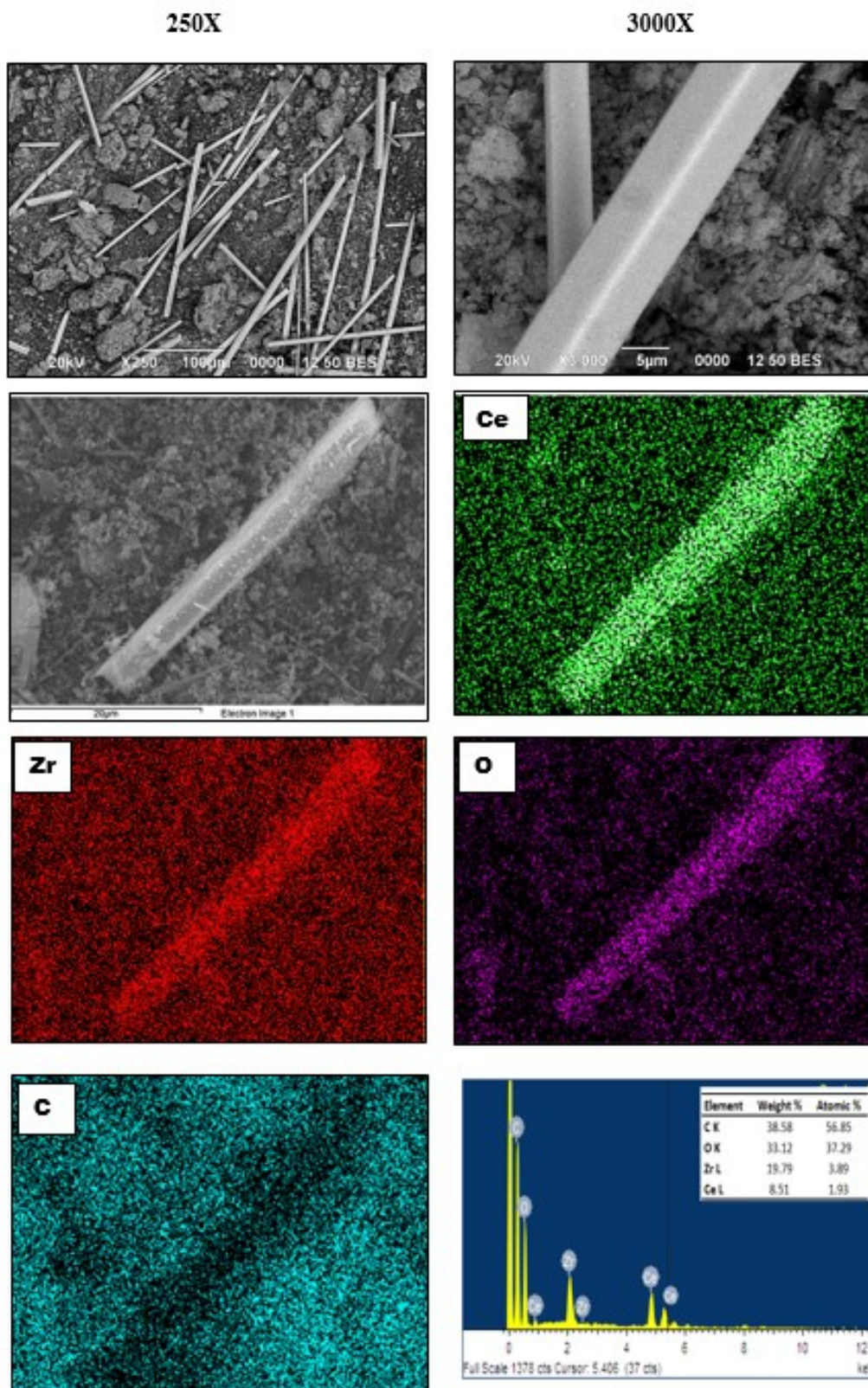


Figure S7. SEM images and SEM-EDS mapping for MOF UiO-66 Ce-Zr

Nitrogen adsorption-desorption

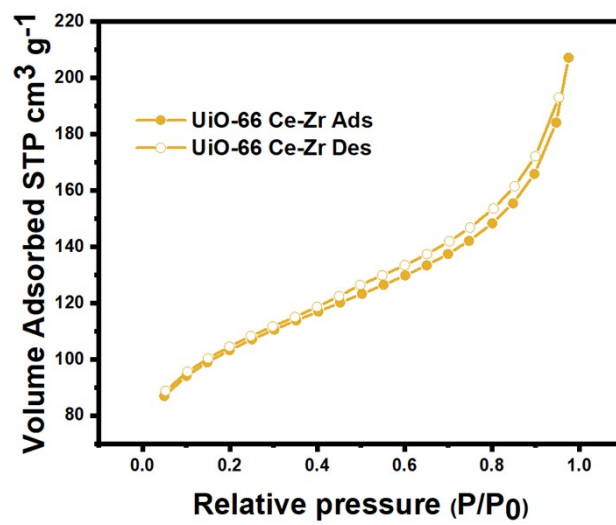
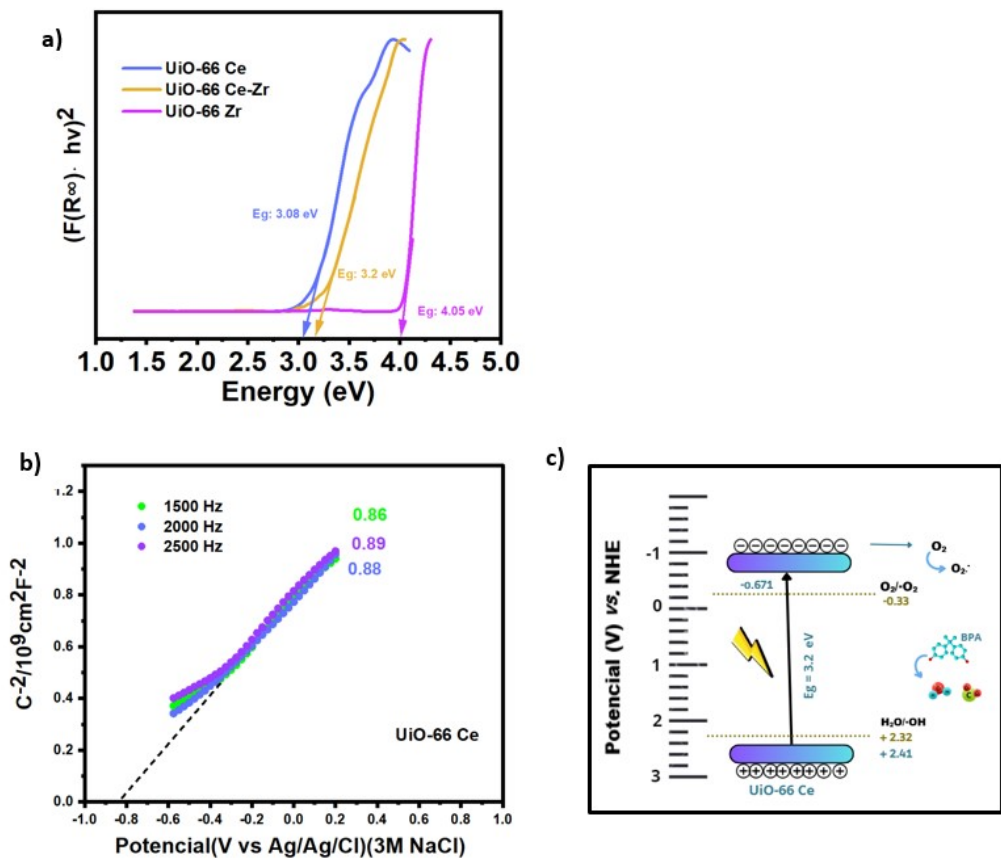


Figure S8. Nitrogen isotherm MOF UiO-66 Ce-Zr: adsorption (Ads) and desorption (Des).

Electrochemical characterization



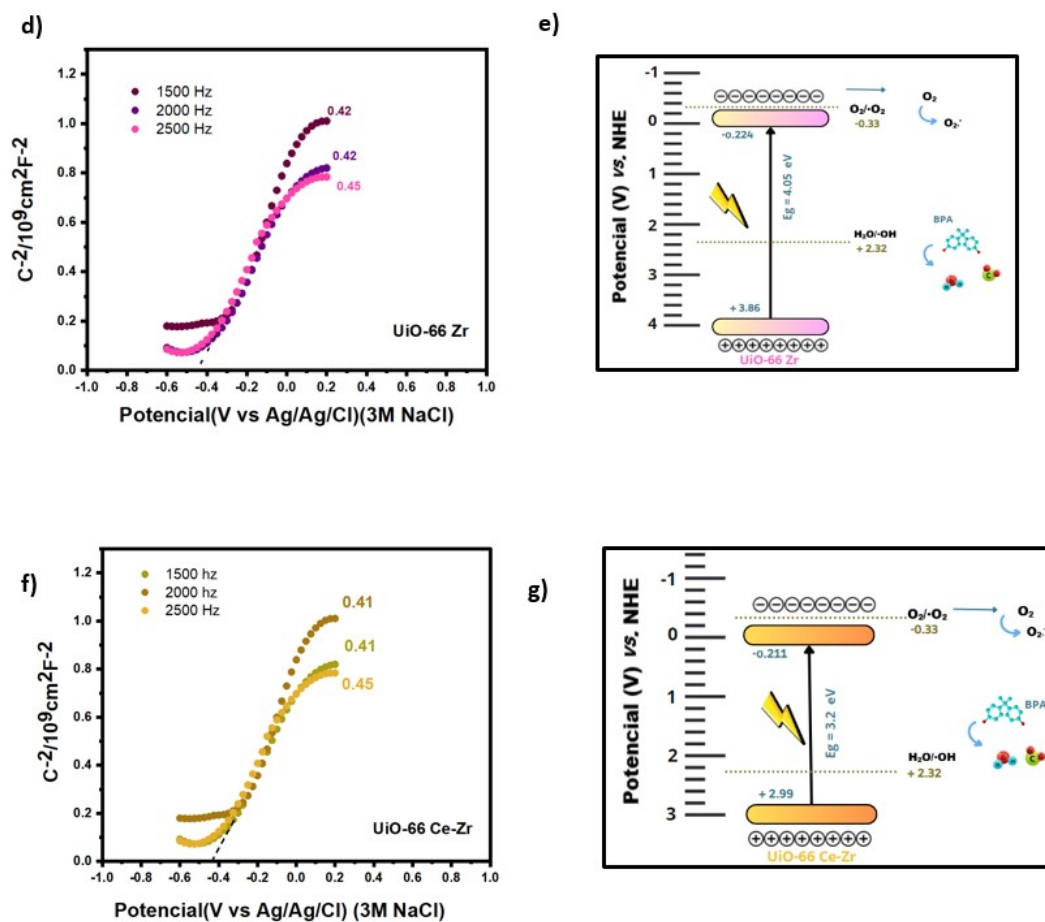


Figure S9 (a) Tauc plots representation and estimated band-gap (E_g) values MOFs UiO-66, (b)-(c) Mott-Schottky curves of prepared at different frequencies (1500, 2000, 2500 Hz) – and electronic band structure of the MOF UiO-66 Ce, (d)-(e) Mott-Schottky curves of prepared at different frequencies (1500, 2000, 2500 Hz) – and electronic band structure of the MOF UiO-66 Zr and (f)-(g) Mott-Schottky curves of prepared at different frequencies (1500, 2000, and 2500 Hz) – and electronic band structure of the MOF UiO-66 Ce-Zr.

BPA degradation analysis

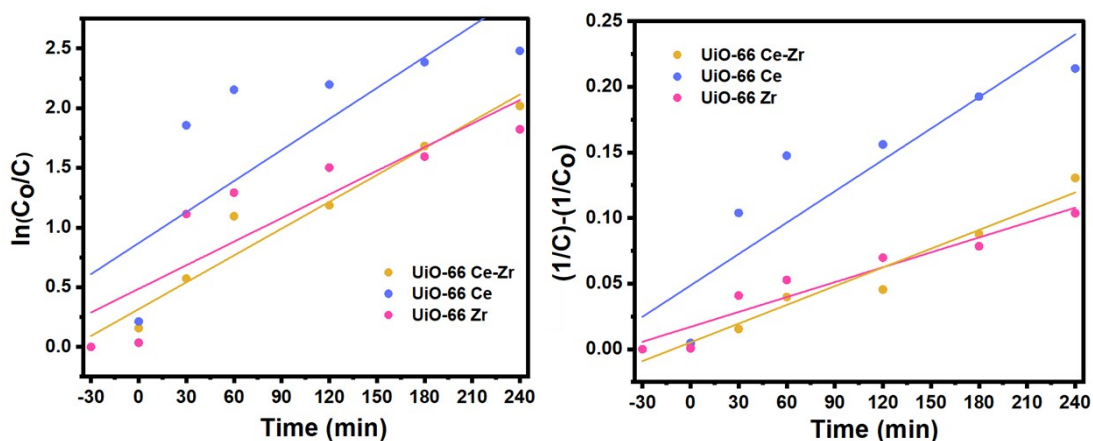


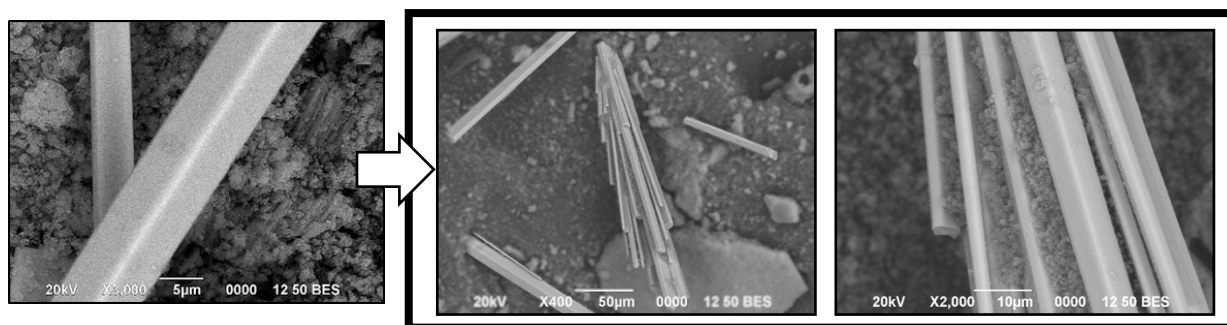
Figure S10. Kinetic studies without and with the lamp of the MOFs UiO-66

Table S2. Parameters of the kinetic models.				
Model	Parameter	Material		
		UiO-66 Ce	UiO-66 Zr	UiO-66 Ce-Zr
	C_0 ($mg \cdot L$)	49.7843	49.8012	49.8012
PFO model	k_1 ($mg \cdot L^{-1} \cdot min^{-1}$)	0.00866	0.00621	0.00749
	R^2	0.664	0.731	0.955
PSO model	C_0 ($mg \cdot L$)	49.7843	49.8012	49.8012
	k_1 ($mg \cdot L^{-1} \cdot min^{-1}$)	0.000813	0.000335	0.000476
	R^2	0.84	0.92	0.960

Table S3. Comparative Table of Different Materials for BPA Degradation				
Photocatalyst	BPA concentration (mg/L)	Reaction time (min)	Degradation efficiency (%)	References
UiO-66 Ce-Zr	50	240	84	This work
UiO-66-NH₂	5	120	16.2	²
Bi₂MoO₆/MIL-88B(Fe)	20	120	54	³
Bi₁₂O₁₇Cl₂/MIL-100(Fe)	20	300	57.4	⁴
UiO-66 Zr	10	120	66	⁵
Mpg-C₃N₄	20	180	52.1	⁶
2% N,B-TiO₂	5	120	79	⁷
BiOI/ZIF-8	10	180	82.5	⁸

Material characterization after BPA degradation

SEM analysis



Before

After

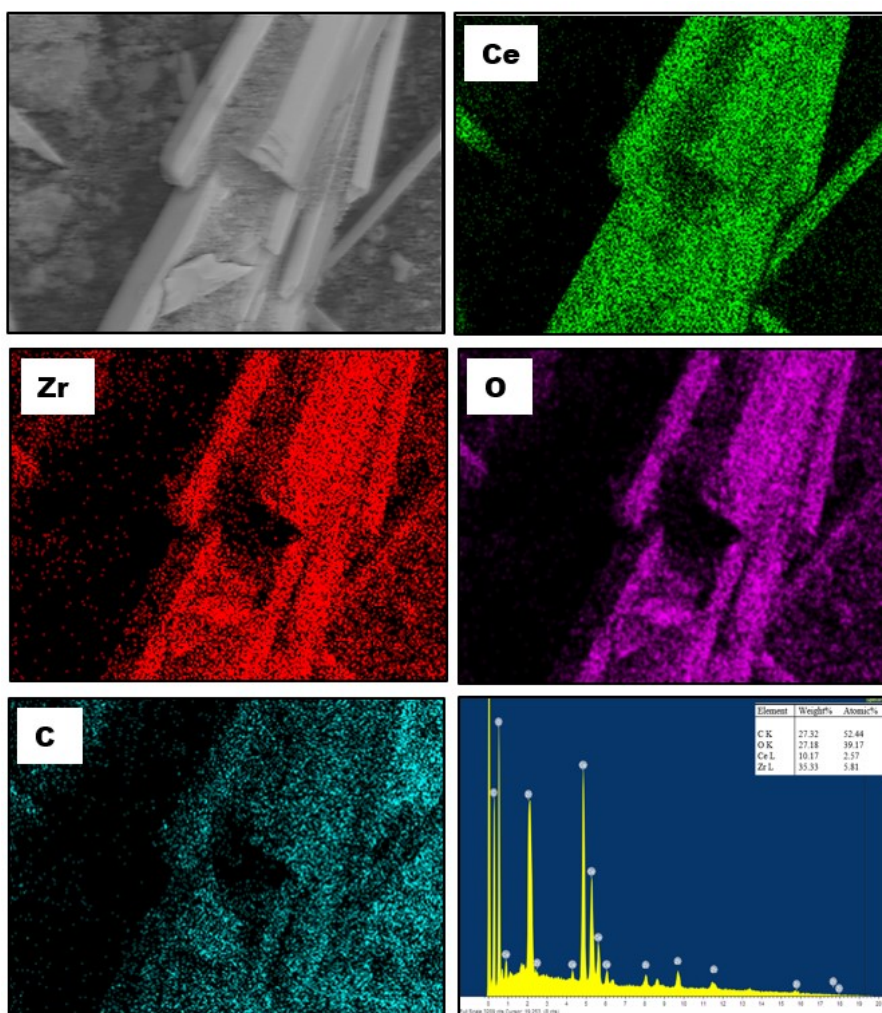


Figure S11. SEM images and SEM MOF UiO-66 Ce-Zr before and after the degradation.

PXRD analysis

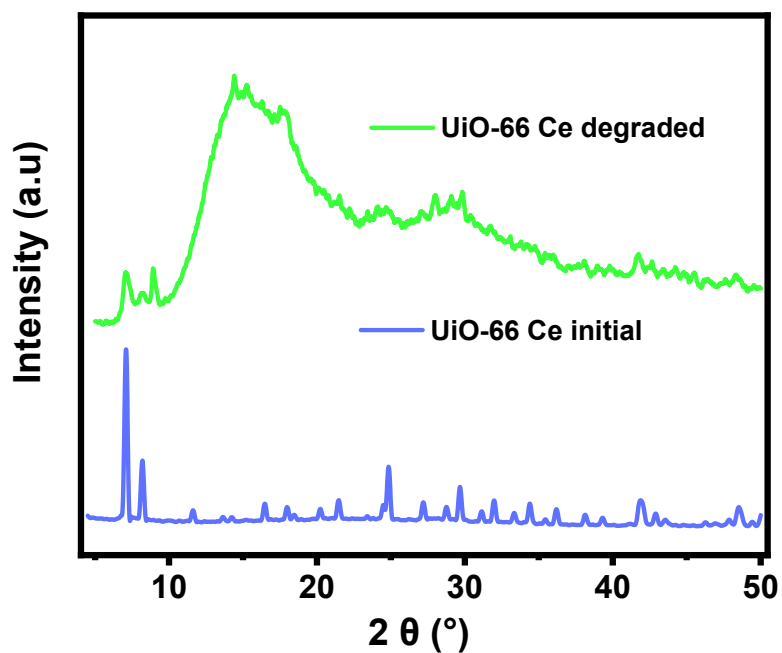


Figure S12. PXRD pattern of MOF UiO-66 Ce initial (blue line) and MOF UiO-66 Ce after degradation (green line).

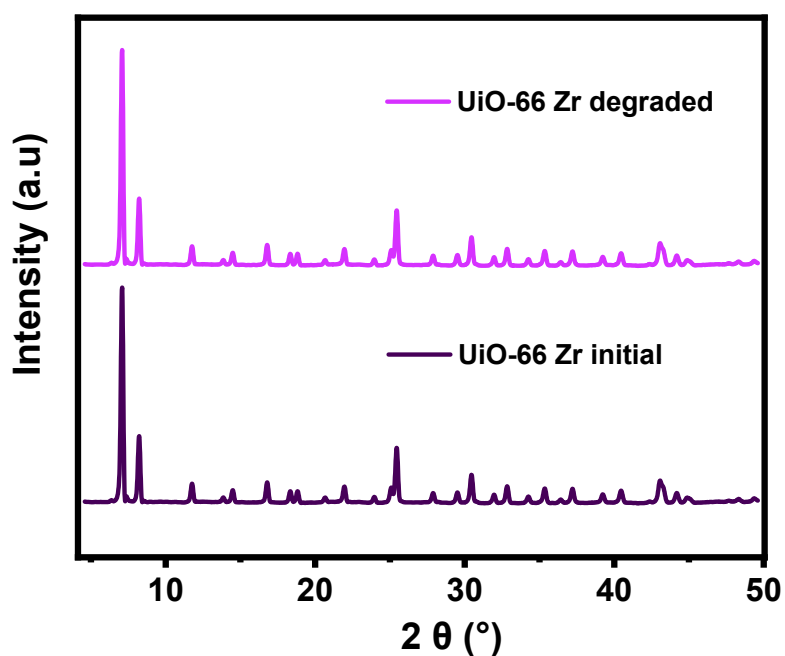


Figure S13. PXRD pattern of MOF UiO-66 Zr initial (dark purple line) and MOF UiO-66 Zr after degradation (purple line).

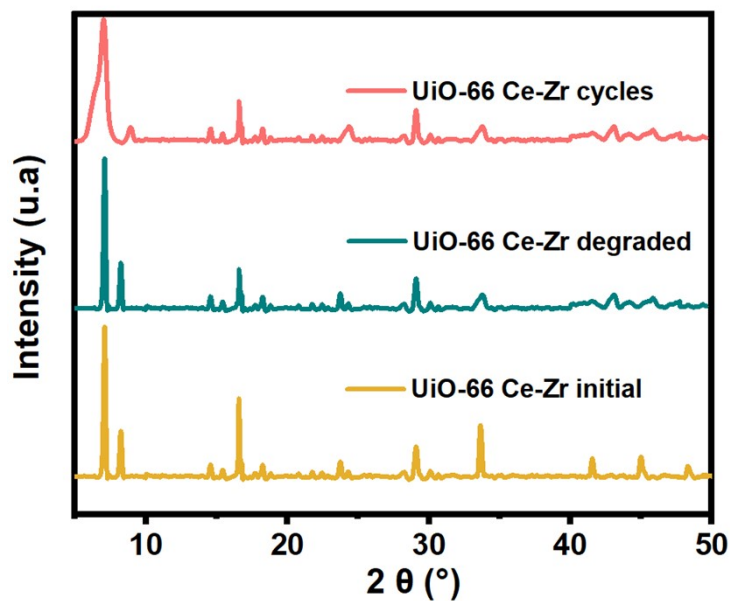


Figure S14. PXRD patterns MOF UiO-66 Ce-Zr initial (yellow line), MOF UiO-66 Ce-Zr degraded (green line) and MOF UiO-66 Ce-Zr after three cycles (red line).

Nitrogen adsorption-desorption after degradation

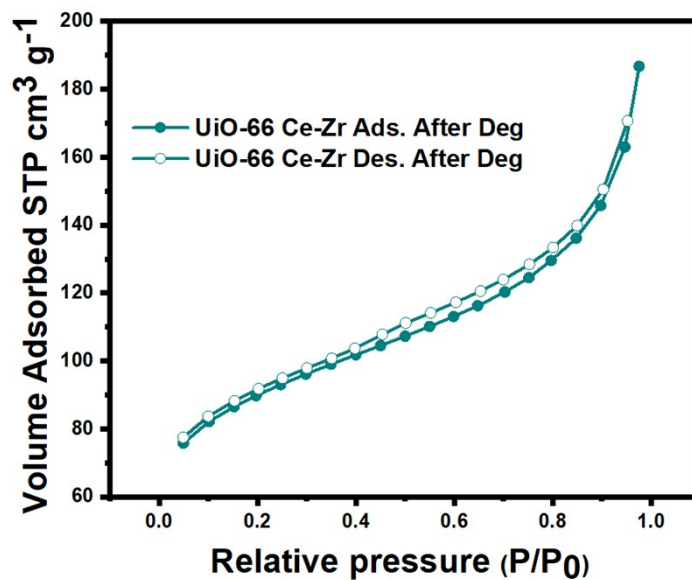


Figure S15. Nitrogen isotherm MOF UiO-66 Ce-Zr: adsorption (Ads) and desorption (Des) after the degradation.

XPS analysis

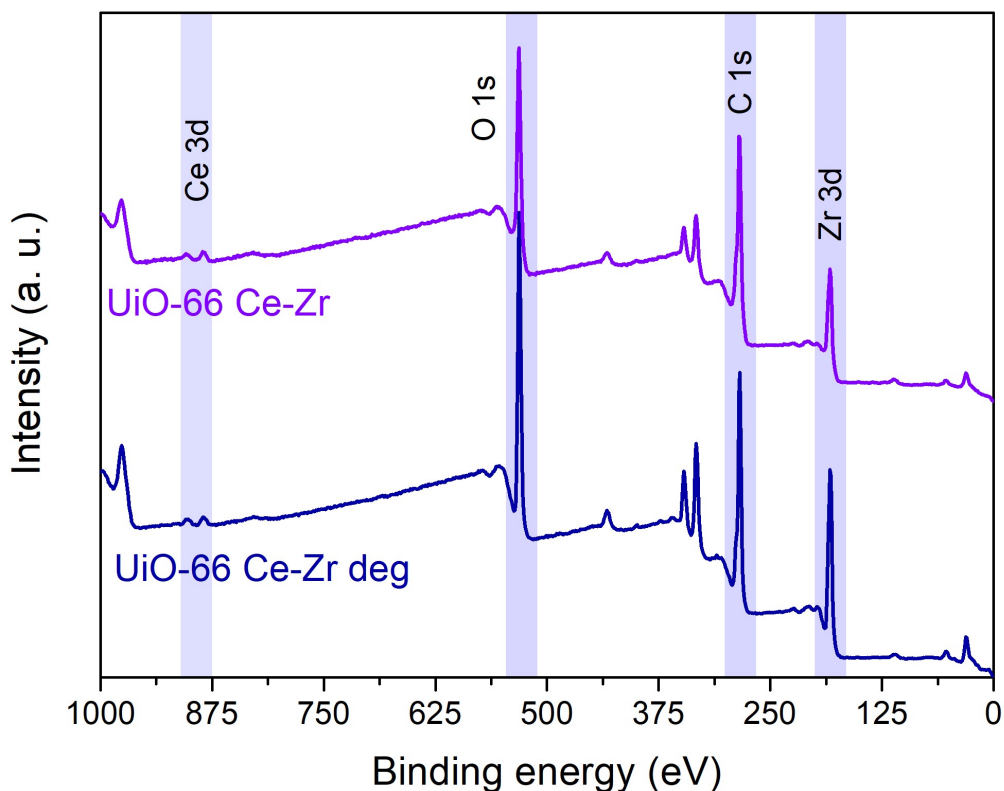


Figure S16. Survey spectra of MOF UiO-66 Ce-Zr, before and after the BPA photodegradation.

Samples	Elements (At. %)				
	C 1s	O 1s	Ce 3d	Zr 3d	N 1s
UiO-66 Ce-Zr	66.6	28.6	0.2	3.0	0.3
UiO-66 Ce-Zr deg	60.4	33.1	0.2	5.6	0.9

Samples	Assignment	E _B (eV)	FWHM (eV)	At. %
UiO-66 Ce-Zr	C1s _{C=C aromatic}	284.7	1.6	64.5
	C1s _{C-OH}	286.1	1.7	15.5
	C1s _{O-C=O}	288.4	1.7	16.5

	C1s π - π^*	289.9	1.8	3.5
UiO-66 Ce-Zr deg	C1s C=C aromatic	284.6	1.5	64.9
	C1s C-OH	285.6	1.5	21.0
	C1s O-C=O	288.6	1.5	10.7
	C1s π - π^*	289.6	1.6	3.4

Table S6. The peak-fitting results of O 1s high-resolution signal of UiO-66 Ce-Zr.

Samples	Assignment	E_B (eV)	FWHM (eV)	At. %
UiO-66 Ce-Zr	O 1s Ce-O, Zr-O	530.1	1.8	14.9
	O 1s O-H, C-O	531.7	1.9	64.0
	O 1s C=O	533.3	1.9	21.1
UiO-66 Ce-Zr deg	O 1s Ce-O, Zr-O	530.1	1.8	19.0
	O 1s O-H, C-O	531.5	1.9	66.2
	O 1s C=O	532.7	1.9	14.8

Table S7. The peak-fitting results of Ce 3d high-resolution signal of UiO-66 Ce-Zr.

Samples	Assignment	E_B (eV)	FWHM (eV)	At. %
UiO-66 Ce-Zr	Ce 3d_{5/2} (v ⁰)	882.5	4.0	19.5
	Ce 3d_{5/2} (v ¹)	886.1	4.0	40.3
	Ce 3d_{3/2} (u ⁰)	901.0	4.0	12.8
	Ce 3d_{3/2} (u ¹)	904.7	4.0	27.4
UiO-66 Ce-Zr deg	Ce 3d_{5/2} (v ⁰)	882.2	3.5	24.7
	Ce 3d_{5/2} (v ¹)	885.8	3.5	35.9
	Ce 3d_{3/2} (u ⁰)	900.7	3.5	15.8
	Ce 3d_{3/2} (u ¹)	904.4	3.5	23.6

Table S8. The peak-fitting results of Zr 3p high-resolution signal of UiO-66 Ce-Zr.

Samples	Assignment	E_B (eV)	FWHM (eV)	At. %
UiO-66 Ce-Zr	Zr 3d_{5/2}	182.6	1.9	51.6
	Zr 3d_{3/2}	184.9	1.9	48.4

UiO-66 Ce-Zr deg	Zr 3d _{5/2}	182.5	1.9	61.4
	Zr 3d _{3/2}	184.8	1.9	38.6

DFT and docking simulations results analysis

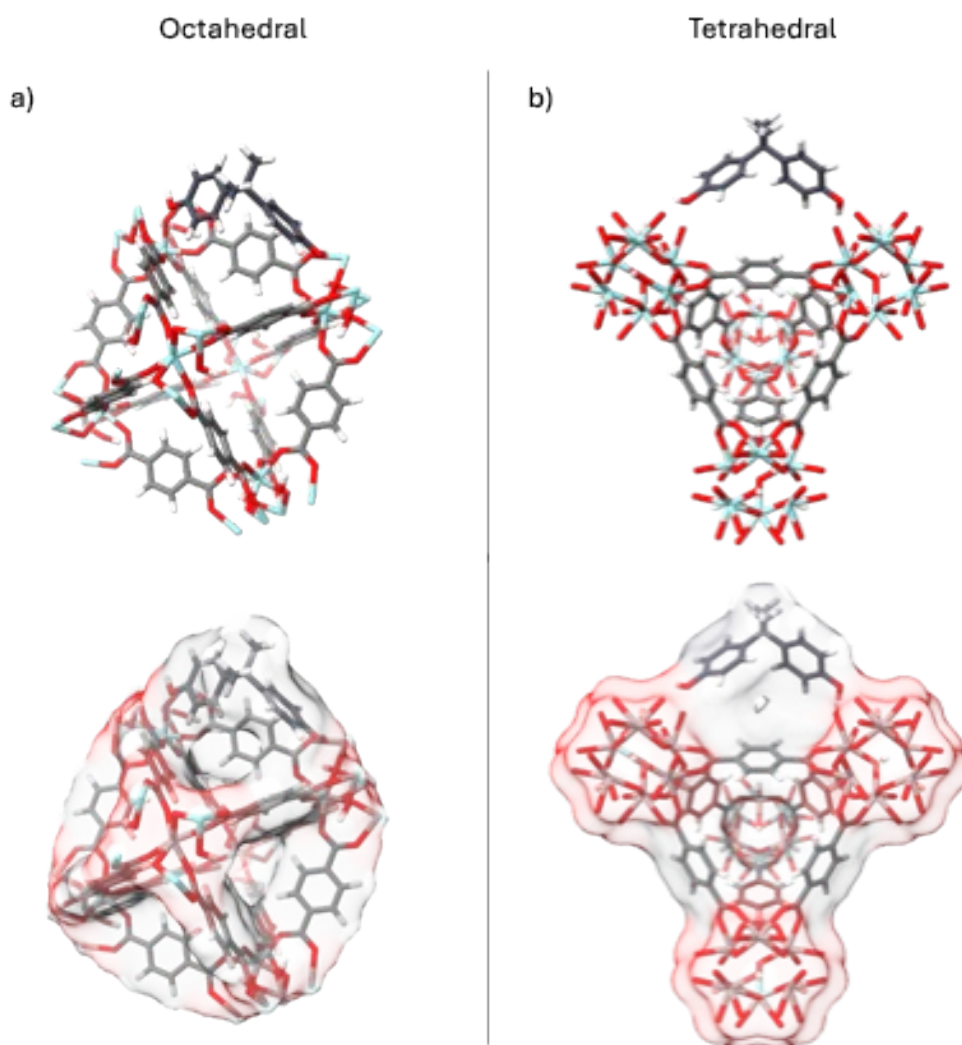


Figure S17. Structural representation of MOF/BPA interactions. (a) Proposed interaction between BPA and UiO-66 in octahedral pore. (b) Proposed interaction between BPA and UiO-66 in tetrahedral pore.

Table S9. Total parameters of volumes calculated with VolMol.

Total Volumes calculated (\AA^3)		
	UiO-66	BPA
Van der Waals volume	2939.96	207.184
Probe excluded void volume	488.056	13.752
Molecular volume (vdw + probe excluded void)	3428.016	220.936
Molecular volume with isolated cavities	3441.32	220.936
Small probe core volume	11.304	0
Small probe shell volume	146.648	0
Small probe occupied volume (core + shell)	157.952	0
Large probe shell volume	7560.68	1323.584

Table S10. Energies reported by DFT study and calculation of binding energy.

Octahedral Pore					
E_i	UiO-66	BPA	→	Adduct	ΔE_i kcal/mol
SCF	-24059745	-458721.84		-24595311	-76843.426
Tetrahedral Pore					
E_i	UiO-66	BPA	→	Adduct	ΔE_i kcal/mol
SCF	-21792178	-458721.84		-22213412	37487.5007

Table S11. Total parameters of surface areas calculated with VolMol.

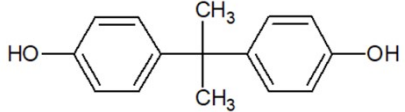
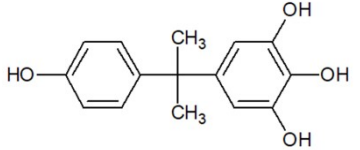
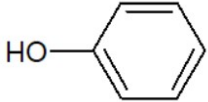
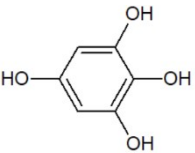
Total Surface Areas calculated (\AA^2)		
	UiO-66	BPA
Van der Waals surface	2437.75147	232.359856
Small probe excluded surface	427.731376	0
Small probe accessible surface (similar to Lee-Richards surface)	69.34754	0
Molecular surface (both probes excluded surface)	2169.72376	220.33068

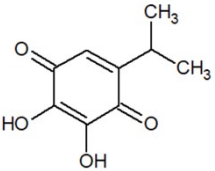

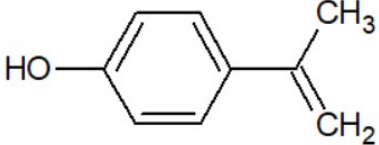
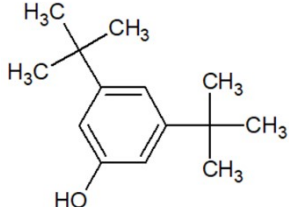
Table S12. Cavities data calculated with VolMol for UiO-66.

Cavity	Occupied Volume (Å ³)	Accessible Volume (Å ³)	Excluded Surface (Å ²)	Accessible Surface (Å ²)	Cavity Type	Cavity Center Coordinates (Å)		
						x	y	z
1	21.664	1.888	58.7557	11.348	Pocket	14.5	3.8	7.2
2	20.624	1.888	56.9695	10.8711	Pocket	10.8	10.4	7.2
3	19.784	1.896	54.6997	10.7459	Pocket	18.2	10.4	7.3
4	17.376	1.2	53.1163	8.67669	Pocket	14.5	8.1	1.2
5	17.216	1.136	44.1072	6.62316	Tunnel	14.5	8.6	10.7
6	16.328	1.104	42.7537	6.80827	Tunnel	14.5	12.9	4.6
7	15.888	1.08	41.4249	6.7227	Tunnel	18.4	6.2	4.4
8	15.768	1.088	41.3877	6.94111	Tunnel	10.6	6.2	4.4
9	4.544	0.008	15.1648	0.2035	Isolated	17.4	12.9	9.1
10	4.536	0.008	15.1648	0.2035	Isolated	11.6	12.9	9.1
11	4.224	0.008	15.0069	0.2035	Isolated	20	8.8	9.1

By-products analysis by UPLC-MS

Table S13. By-products analysis with diferen m/z.

<i>Compound</i>	<i>Molecular Structure</i>	<i>Molecular formula</i>	<i>Molecular Mass (M)^a (g/mol)</i>	<i>(M-H)⁺ (m/z)</i>	<i>t_R (min)</i>	<i>Ref.</i>
BPA		C₁₅H₁₆O₂	228.29	227.29	6.02 6.67	9
5-[2-(4-hydroxyphenyl)propan-2-yl]benzene-1,2,3-triol		C₁₅H₁₆O₄	260.29	259.3	6.67	
phenol		C₆H₆O	94.1	93.2	0.845	
benzene-1,2,3,5-tetrol		C₆H₆O₄	142.1	141.1	0.845	

2,3-dihydroxy-5-(propan-2-yl)cyclohexa-2,5-diene-1,4-dione		C₉H₁₀O₄	182.1	181.1	0.845 6.02 6.67	
(2Z)-but-2-enedioic acid		C₄H₄O₄	116.05	115.01	0.530	
4-(prop-1-en-2-yl)phenol		C₉H₁₀O	134.17	133	6.02 6.67	10
3,5-di-tert-butylphenol		C₁₄H₂₂O	206.32	205.12	0.845 6.02 6.67	11

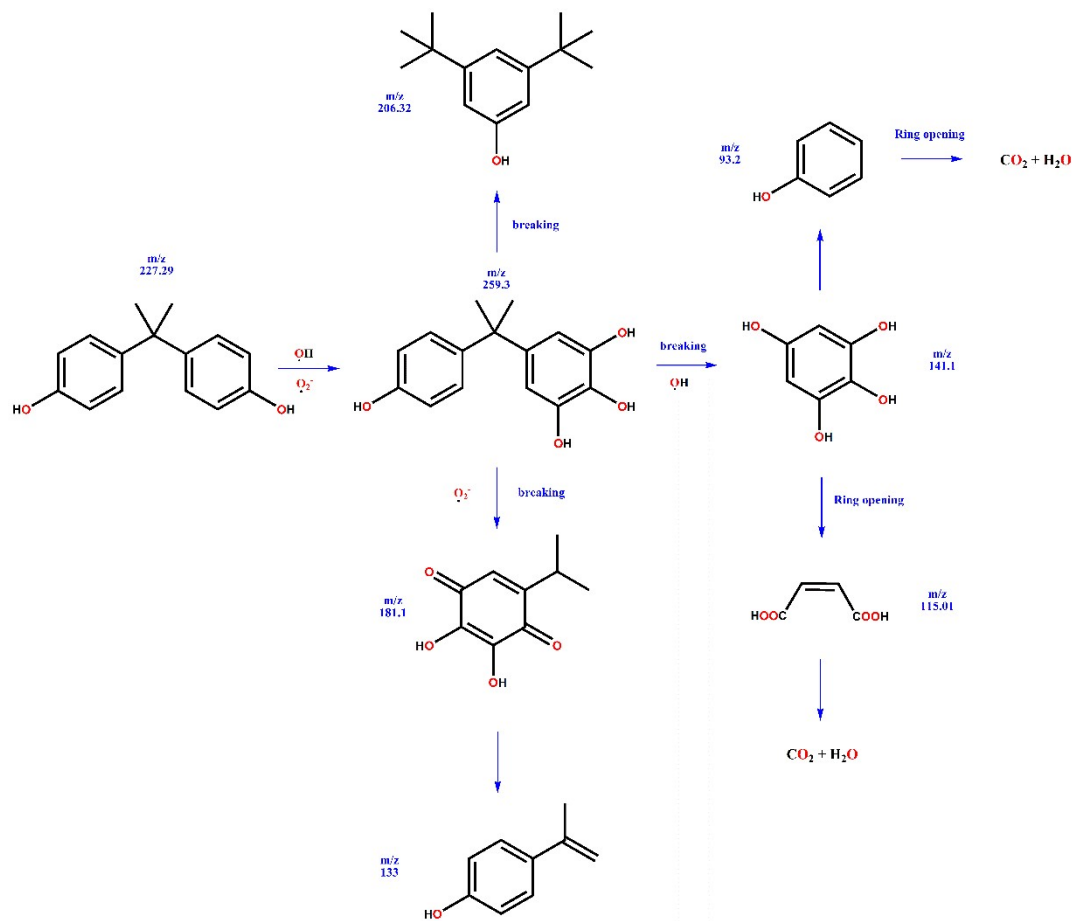
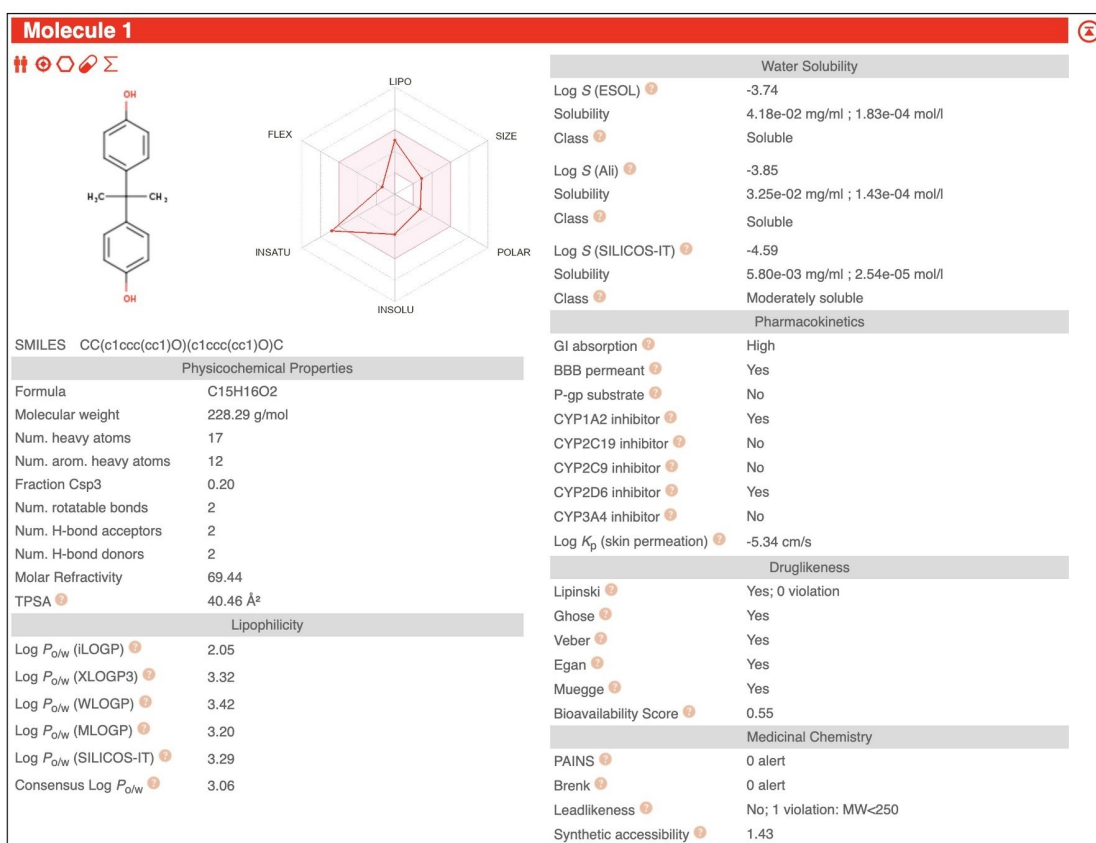
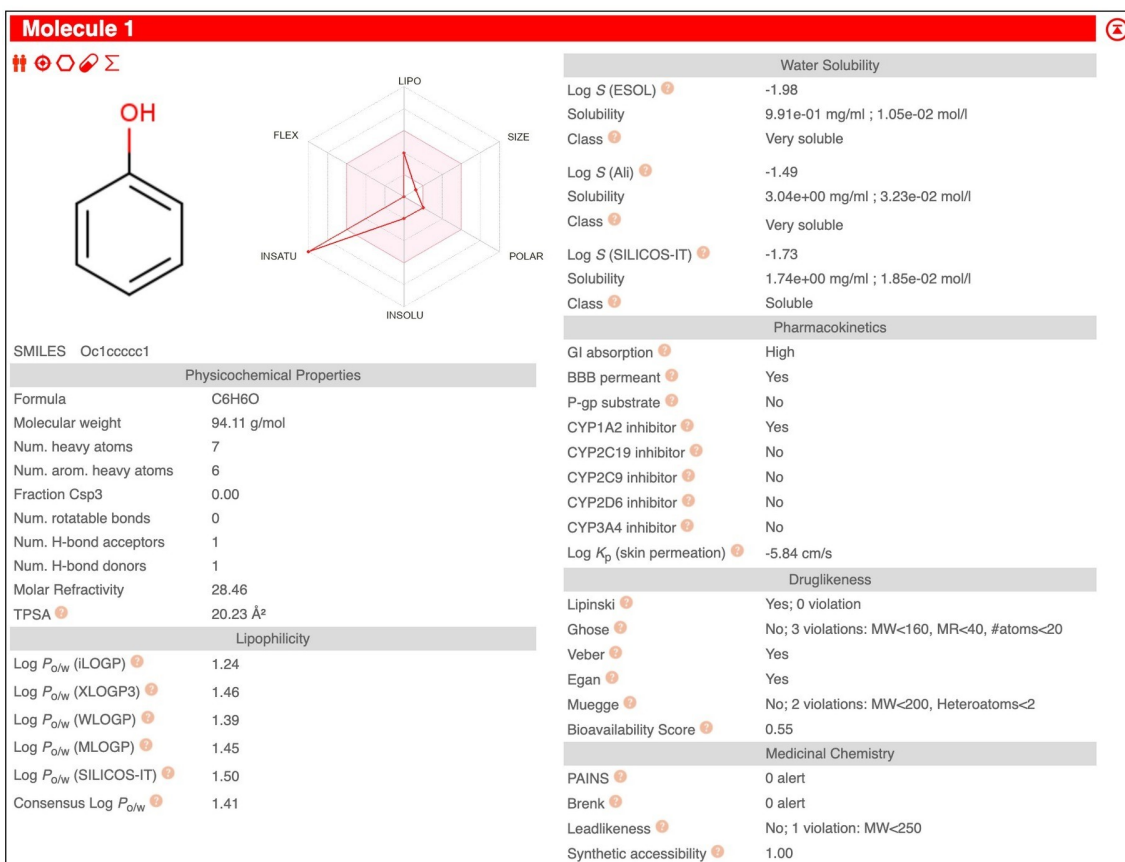
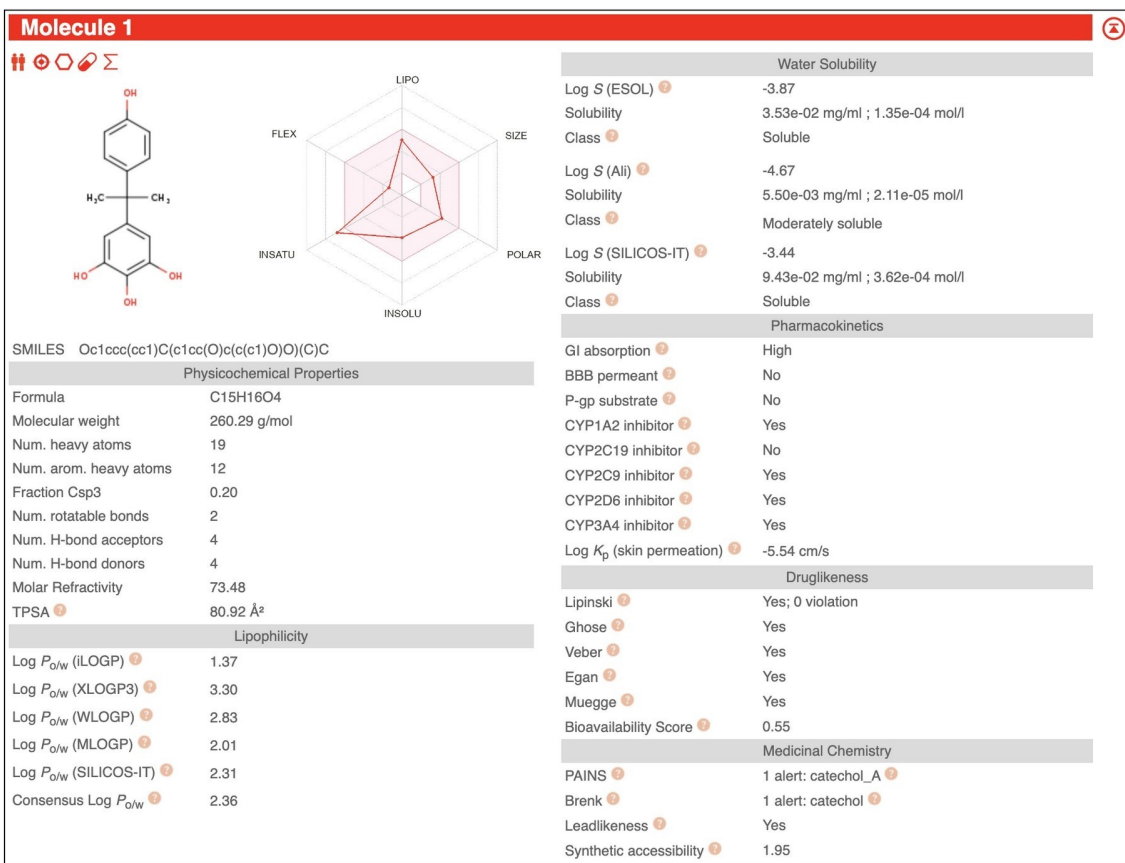
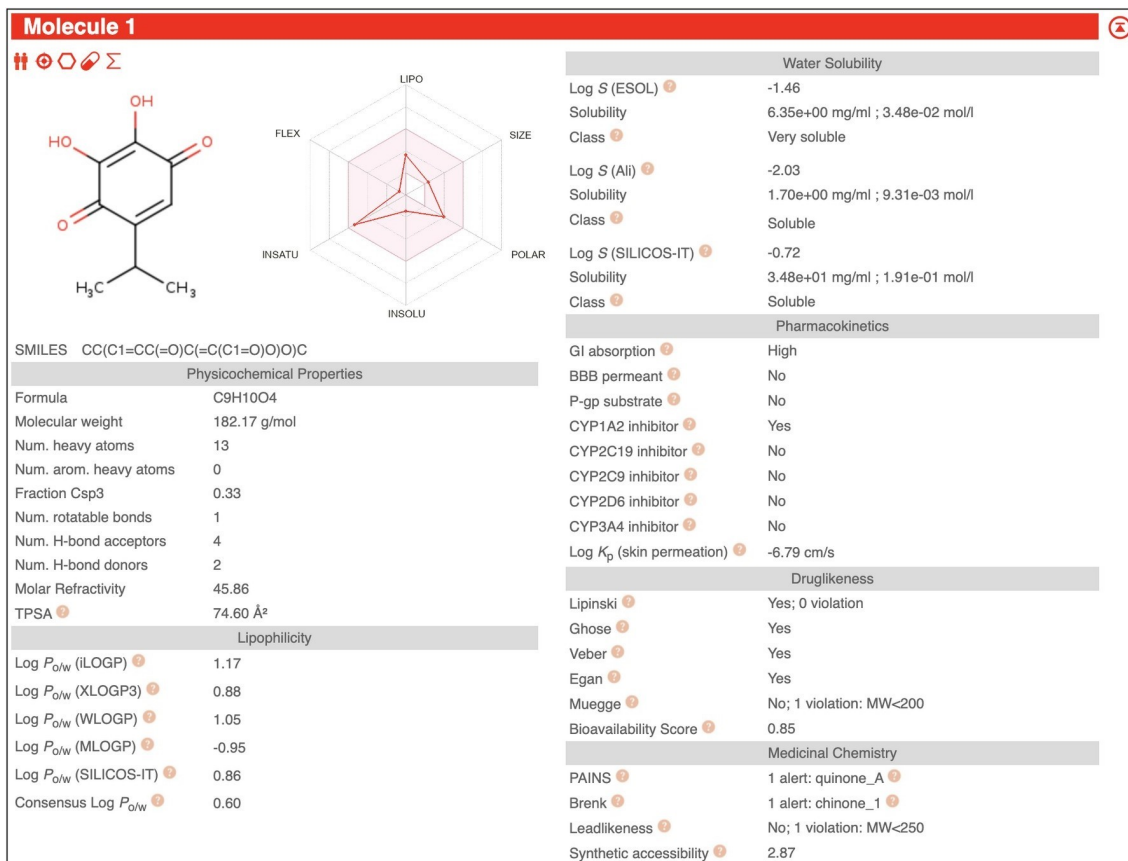
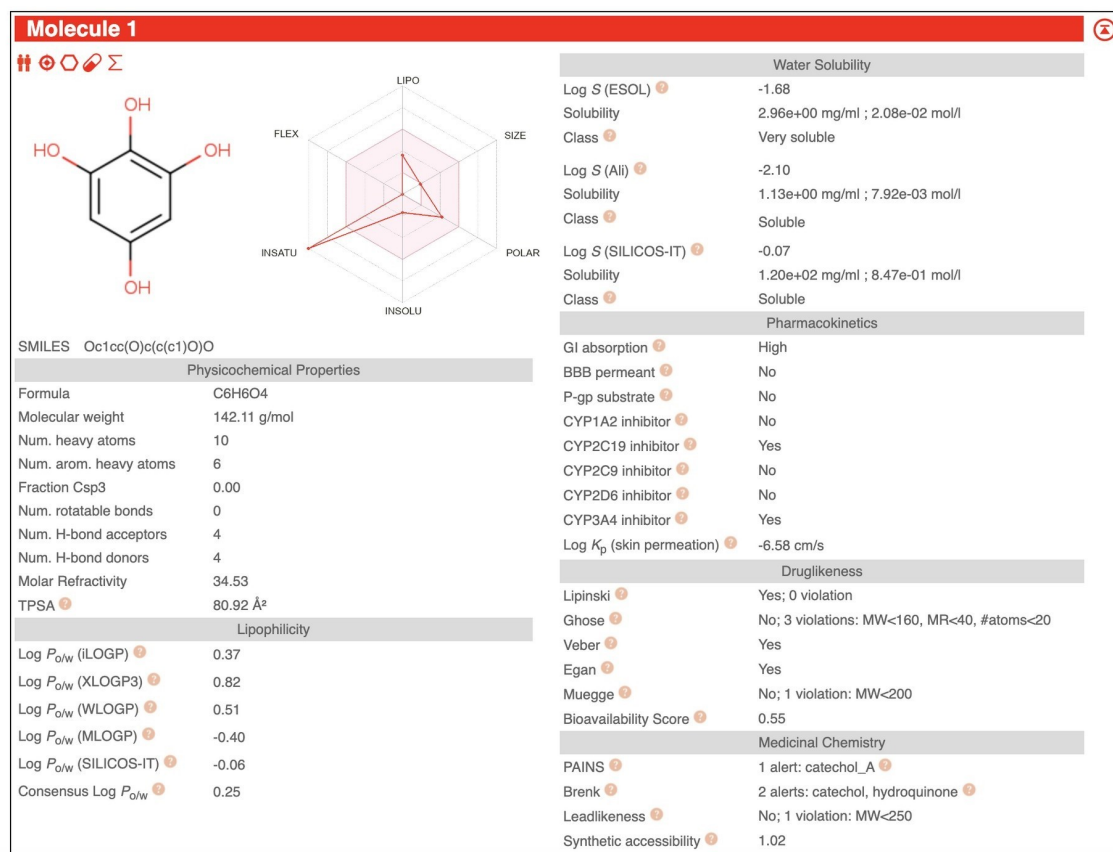


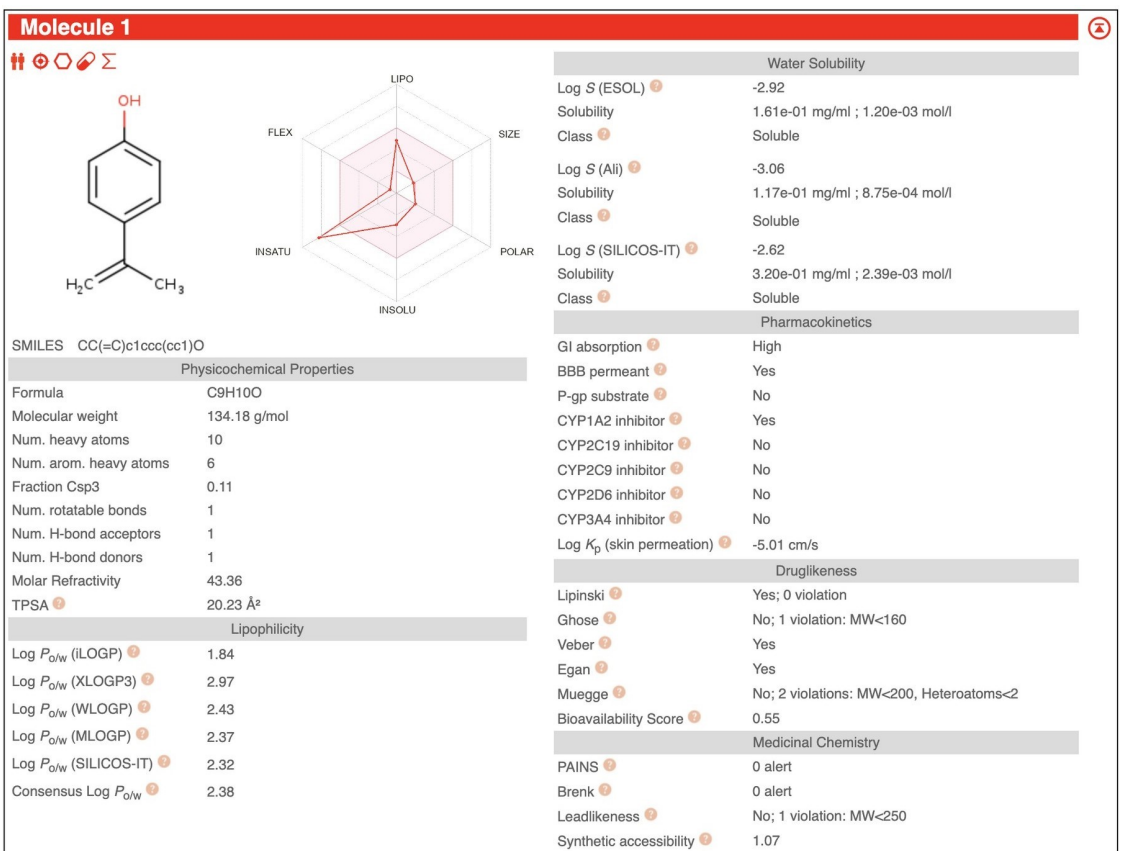
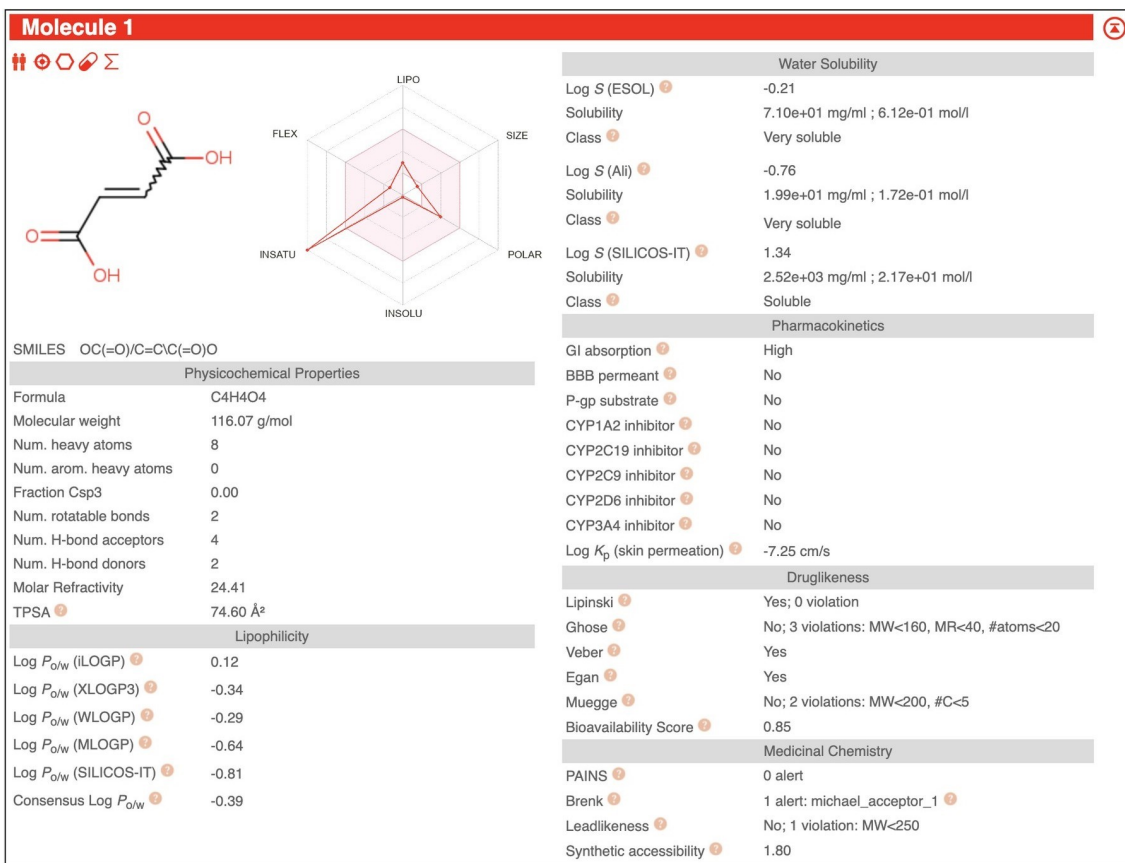
Figure S18. Reaction pathway for the photocatalytic degradation of bisphenol A with UiO-66 Ce-Zr illuminated with UV light.

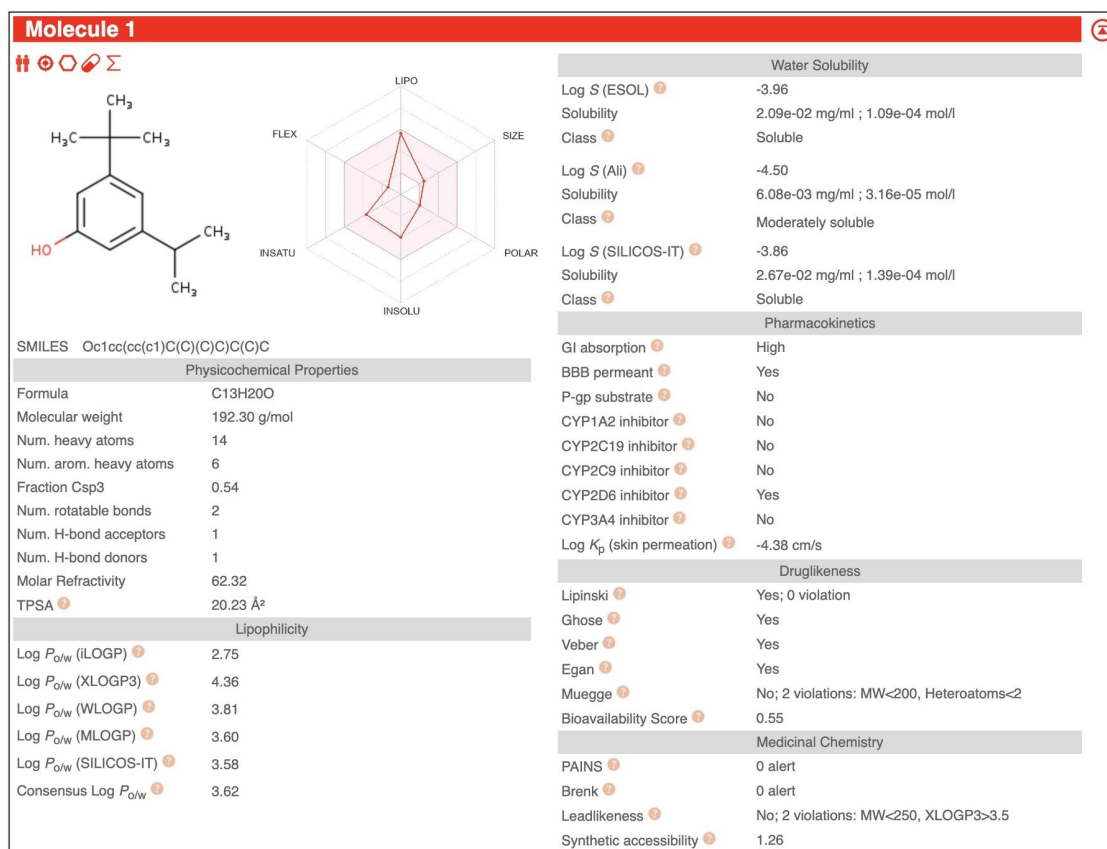
Toxicology in-silico study of degradation products











S3. References

- 1 P. H. M. Andrade, C. Volkringer, T. Loiseau, A. Tejada, M. Hureau and A. Moissette, *Applied Materials Today*, 2024, **37**, 102094.
- 2 Y.-X. Li, X. Wang, C.-C. Wang, H. Fu, Y. Liu, P. Wang and C. Zhao, *Journal of Hazardous Materials*, 2020, **399**, 123085.
- 3 K. Zhao, Z. Zhang, Y. Feng, S. Lin, H. Li and X. Gao, *Applied Catalysis B: Environmental*, 2020, **268**, 118740.
- 4 C. Zhao, J. Wang, X. Chen, Z. Wang, H. Ji, L. Chen, W. Liu and C.-C. Wang, *Science of The Total Environment*, 2021, **752**, 141901.
- 5 S. Feng, R. Wang, S. Feng, Z. Zhang and L. Mao, *Res Chem Intermed*, 2019, **45**, 1263–1279.
- 6 C. Chang, Y. Fu, M. Hu, C. Wang, G. Shan and L. Zhu, *Applied Catalysis B: Environmental*, 2013, **142–143**, 553–560.
- 7 W. H. M. Abdelraheem, M. K. Patil, M. N. Nadagouda and D. D. Dionysiou, *Applied Catalysis B: Environmental*, 2019, **241**, 598–611.
- 8 W. Zheng, S. Feng, C. Shao, G. Zhu, Z. Ni, J. Sun and X. Huang, *Res Chem Intermed*, 2020, **46**, 2951–2967.
- 9 J. C. C. Da Silva, J. A. Reis Teodoro, R. J. D. C. F. Afonso, S. F. Aquino and R. Augusti, *Rapid Comm Mass Spectrometry*, 2014, **28**, 987–994.
- 10 Y. Wang, K. Hu, Z. Yang, C. Ye, X. Li and K. Yan, *Front. Bioeng. Biotechnol.*, 2021, **8**, 616780.
- 11 X. Li, Z. Wang, B. Zhang, A. I. Rykov, M. A. Ahmed and J. Wang, *Applied Catalysis B: Environmental*, 2016, **181**, 788–799.